Geophysical Research Letters

RESEARCH LETTER
10.1029/2019GL084099

Using Overshooting Top Area to Discriminate Potential for Large, Intense Tornadoes

G. R. Marion[1], R. J. Trapp[1], and S. W. Nesbitt[1]

[1]Department of Atmospheric Sciences, University of Illinois at Urbana-Champaign, Urbana, IL, USA

Key Points:
- There is a strong relationship of overshooting top area to tornado EF rating in tornadic thunderstorms
- This relationship holds for different storm morphologies, seasons, and geographic locations
- The overshooting top area method shows promise in operational applications

Correspondence to:
G. R. Marion,
gmarion2@illinois.edu

Citation:
Marion, G. R., Trapp, R. J., & Nesbitt, S. W. (2019). Using overshooting top area to discriminate potential for large, intense tornadoes. *Geophysical Research Letters*, *46*, 12,520–12,526. https://doi10.org/1029/2019GL084099

Received 13 JUN 2019
Accepted 9 OCT 2019
Accepted article online 18 OCT 2019
Published online 5 NOV 2019

Abstract Recent work established strong links between storm updraft width and the tornado intensity, suggesting that updraft width could be used to gauge potential tornado intensity. It was also posited that overshooting top area (OTA) could be used as an analog for updraft width and, thus, as a means to assess potential tornado intensity in observed storms. The implementation of new high-resolution GOES-R series satellites presents a unique opportunity to investigate these findings in severe weather observations. Herein, a method using GOES-16 longwave infrared satellite data to quantify OTA of tornadic storms is explored. A comparison between observed tornado strength and OTA yields a strong correlation ($R^2 = 0.54$). These results show the potential of these quantifications to be used with real-time observations of tornadic storms, irrespective of storm mode, seasonality, or geographic location, allowing forecasters to determine which storms pose the highest risk to life and property.

Plain Language Summary Identifying storms capable of producing strong tornadoes remains a focus of severe weather research due to their significant impacts to life and property. Recent advancements in satellite observations present new opportunities to develop methods for identifying these storms. Using satellite imagery of the top of severe thunderstorms, a strong relationship is identified between the size of the imprint of the storm's updraft and the strength of the tornado that may develop within it. This information might be used by meteorologists to identify storms with the highest potential to produce violent tornadoes and to communicate better the risk posed by them to the public.

1. Introduction

Identification of cloud top features in satellite imagery has long been used in methods of severe weather detection. In particular, the presence of overshooting tops (OTs), which are associated with intense deep convection extending into the relatively warm lower stratosphere (Adler & Fenn, 1979), have been linked to flash flooding, large hail, strong winds, and tornadoes (Bedka et al., 2010; Dworak et al., 2012; Negri & Adler, 1981; Reynolds, 1980). Severe-storm occurrence, particularly hail occurrence, has additionally been linked to the so-called "enhanced-V" signature (e.g., Adler et al., 1981; Adler et al., 1985; Brunner et al., 2007; Fujita, 1982; Homeyer et al., 2014; McCann, 1983; Mills & Astling, 1977; Negri, 1982), which is related to upper-level divergence about robust convective updrafts. More recently, "above-anvil cirrus plumes" (e.g., Bedka et al., 2018; Homeyer et al., 2017), which are associated with an injection of cloud particles into the lower stratosphere, have also been associated with severe thunderstorms.

The use of cloud top characteristics to anticipate severe-weather *intensity* in addition to occurrence has not yet been well demonstrated, especially for tornadoes, but the work of Trapp et al. (2017) suggests a possible method toward this end. Trapp et al. (2017) applied conservation of circulation principles to the tornado-damage-track analysis of Brooks (2004) to hypothesize that larger, stronger tornadoes are more likely to form out of larger mesocyclones, that is, larger rotating updrafts. They found strong support of this hypothesis in a series of idealized supercell simulations (see also Trapp et al., 2018), which were also used to identify dynamic links between the storm's midlevel updraft and the near-surface tornadic-vortex intensity. The simulations and physical reasoning additionally indicated a robust correlation between midlevel updraft area and the horizontal area of its associated OT (overshooting top area; OTA), identified as contiguous areas of cloud top temperatures colder than 5 K minus the tropopause temperature. They suggested that satellite imagery of OTs could be used in real time to identify storms with large updrafts and, thus, the highest potential to produce strong, damaging tornadoes. The work herein is presented as an initial evaluation of this proposed relationship between OTA and tornado intensity.

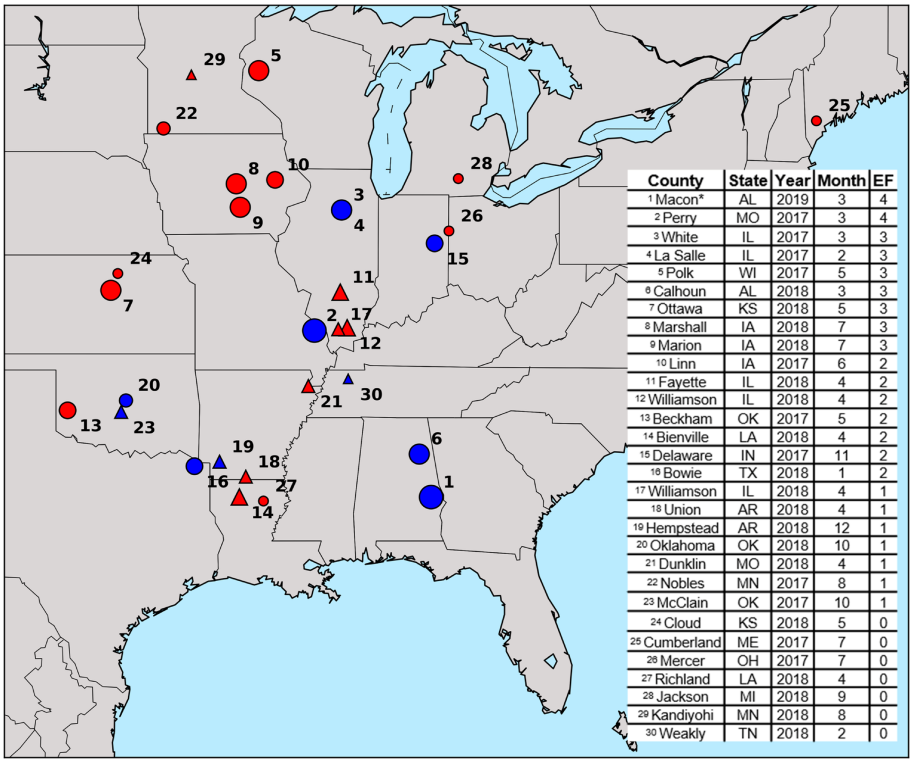

	County	State	Year	Month	EF
1	Macon*	AL	2019	3	4
2	Perry	MO	2017	3	4
3	White	IL	2017	3	3
4	La Salle	IL	2017	2	3
5	Polk	WI	2017	5	3
6	Calhoun	AL	2018	3	3
7	Ottawa	KS	2018	5	3
8	Marshall	IA	2018	7	3
9	Marion	IA	2018	7	3
10	Linn	IA	2017	6	2
11	Fayette	IL	2018	4	2
12	Williamson	IL	2018	4	2
13	Beckham	OK	2017	5	2
14	Bienville	LA	2018	4	2
15	Delaware	IN	2017	11	2
16	Bowie	TX	2018	1	2
17	Williamson	IL	2018	4	1
18	Union	AR	2018	4	1
19	Hempstead	AR	2018	12	1
20	Oklahoma	OK	2018	10	1
21	Dunklin	MO	2018	4	1
22	Nobles	MN	2017	8	1
23	McClain	OK	2017	10	1
24	Cloud	KS	2018	5	0
25	Cumberland	ME	2017	7	0
26	Mercer	OH	2017	7	0
27	Richland	LA	2018	4	0
28	Jackson	MI	2018	9	0
29	Kandiyohi	MN	2018	8	0
30	Weakly	TN	2018	2	0

Figure 1. Map of the cases used, with red and blue markers indicating "warm" (April–September) and "cool" (October–March) season events, respectively, and circle and triangle markers indicating supercell and quasi-linear convective system storm mode cases. Individual marker size corresponds to each tornado's rating (higher ratings being larger), as summarized in the inset table (the asterisk denotes the case for which the rating was preliminary at time of analysis).

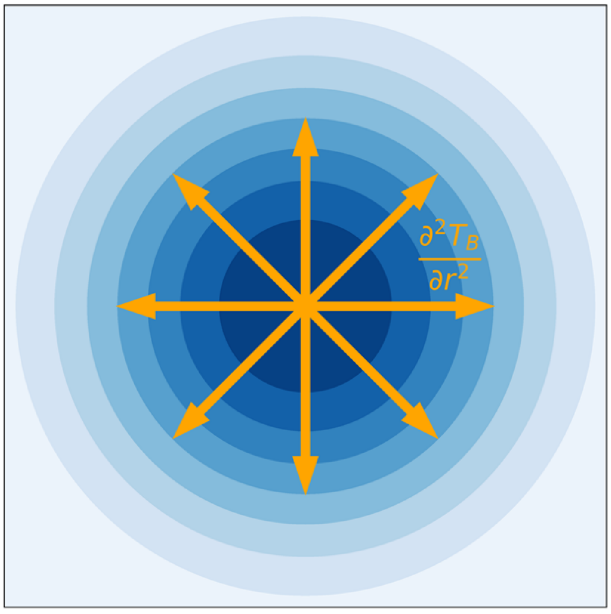

Figure 2. Brightness temperature (T_B) field associated with a hypothetical overshooting top. Darker shading indicates relatively lower T_B. The orange arrows depict the eight radials along which the 1-D Laplacian of T_B is computed. The overshooting top edge is equated with the point along the radial where the 1-D Laplacian first becomes 0.

The evaluation of OTA is facilitated by the advent of the new GOES-R series satellites (Goodman et al., 2012), which offer comparably higher spatial and temporal resolution to past geostationary satellite observations. Higher spatial resolution provides the ability to more exactly quantify OTA. Additionally, the higher temporal resolution allows for better sampling of the rapid evolution of intense convective storms. GOES-16, viewing severe weather-prone regions of the eastern and central United States, has now been operational for more than 2 years, allowing a test of OTA-tornado relationships.

Herein, we investigate whether the quantification of OTA in GOES-16 longwave infrared (LWIR) satellite imagery provides a means for distinguishing storms with the highest potential to produce strong, damaging tornadoes. Such tornadoes—those with Enhanced Fujita (EF) rating of EF3 and greater—result in a disproportionate number of fatalities (Ashley, 2007), thus motivating efforts to identify them. In section 2, the tornado case selection and OTA quantification methodology is outlined. Section 3 summarizes the results of this analysis. Finally, in section 4, the broader applicability of this approach, along with future work, is discussed.

2. Methodology

The analysis is performed using the 5-min GOES-16 Channel 14 LWIR data available during the GOES-16 operational period, which began 28 February 2017. Note that the use of 1-min data would be preferable, but these data are available only within rapid-scan mesoscale sectors and

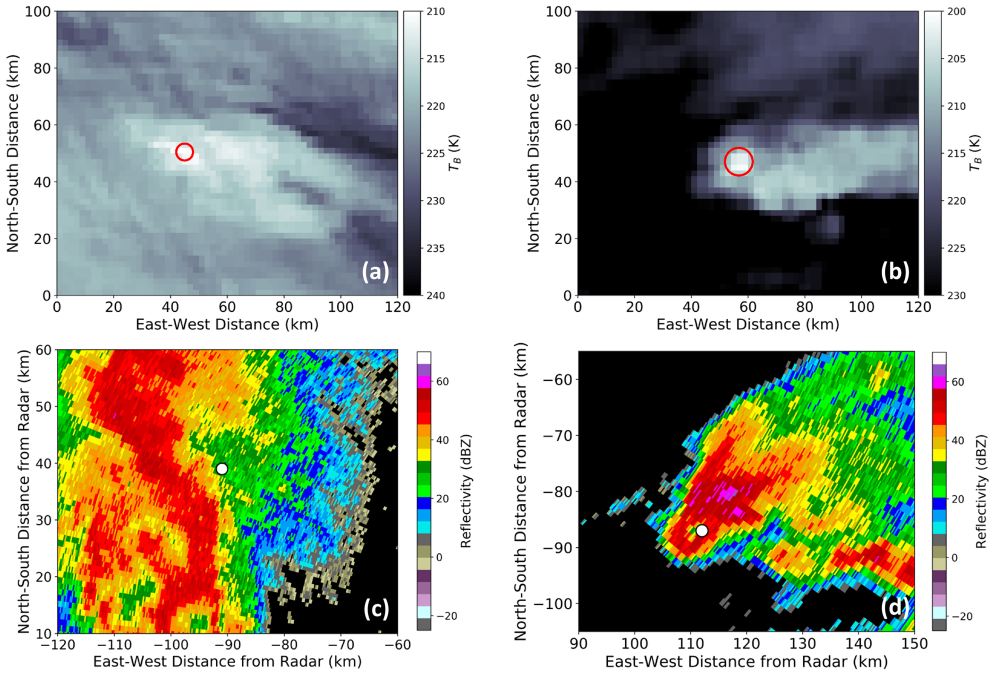

Figure 3. Longwave infrared satellite imagery and corresponding radar images of the (a, c) EF0 and (b, d) EF4 tornadic storms that occurred on 3 August 2018 at 2332 UTC and 1 March 2017 at 0237, respectively. Overlaid red circles in (a) and (b) indicate the approximate size of each overshooting top in the satellite images, and white markers in (c) and (d) indicate the approximate location of the overshooting top in the radar images (note the color scale differences for each satellite image).

thus are associated with fewer tornado cases. Nonetheless, because the 5- and 1-min data have the same spatial resolution, the statistical relationships identified in the 5-min data are directly applicable to these rapid-scan data. The case selection is facilitated by the National Centers for Environmental Information Storm Event Database (https://www.ncdc.noaa.gov/stormevents/), which is used to identify cases with varying seasonality (i.e., "cool" season: October through March, and "warm" season: April through September), geographic location, and storm morphology (i.e., supercell thunderstorm and quasi-linear convective system [QLCS], as identified following the criteria of Smith et al., 2012; Trapp et al., 2005). A summary of these cases is provided in Figure 1. Here we note that although Trapp et al. (2017) focused on supercell thunderstorms, inclusion of QLCS-generated tornadoes allows for a test of the broader applicability of the OTA-tornado relationship; such applicability is indeed suggested by ongoing work aimed at understanding the genesis of QLCS tornadoes. An intentional effort is also made to select equal numbers of cases rated EF0–EF3. Due to the relative scarcity of high-end (EF4, EF5) tornadoes during the GOES-16 operational period thus far, only two EF4 cases and no EF5 cases are included. Also, to help ensure the legitimacy of EF0 cases (e.g., see Doswell et al., 2009; Edwards et al., 2013), we require that they be associated with a nonzero estimation of property damages. In the regression analysis presented in section 3, we used the estimated maximum wind speed of the tornado, if included in the report. For tornado reports in which no wind speed estimate was given (15 of the 30 used here), the average of the respective EF rating wind range was used (see Cohen et al., 2018).

OTA quantification first requires the identification of an OT. Our method for OT identification basically follows that of Bedka and Khlopenkov (2016), which searches for quasi-horizontal (storm top) gradients in brightness temperature (T_B). Specifically, the method equates edges of the OT with inflection points in the T_B field. To illustrate, consider the hypothetical OT in Figure 2. Beginning at the location of the minimum T_B (T_{Bmin}), we assemble a scalar array of T_B values along a radial extending from this point. The 1-D second derivative along the radial ($\frac{d^2T_B}{dr^2}$) is then calculated using a simple forward finite difference approximation. The edge of the OT along this radial is defined as the first point where $\frac{d^2T_B}{dr^2} \leq 0$. This process is repeated along seven other radials, identifying the edge of the overshoot in each direction. The OTA is then calculated assuming the OT is circular in shape, so that $OTA = \pi r_m^2$, where r_m^2 is the length of the mean radial.

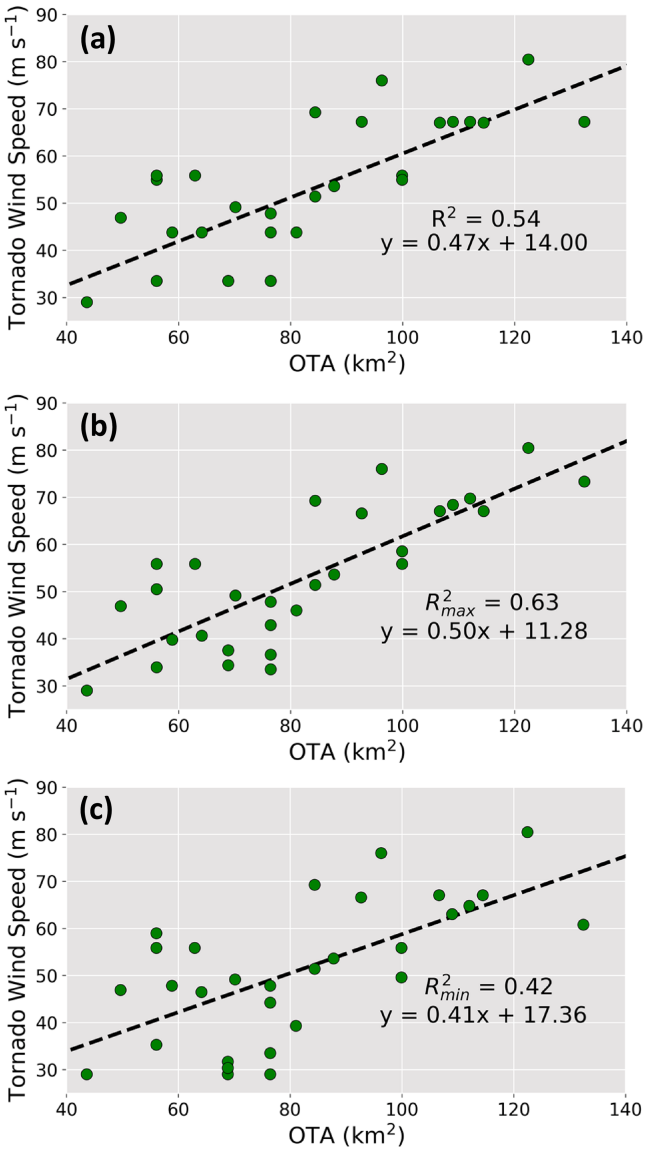

Figure 4. (a,b,c) Scatter plots of overshooting top area (OTA; km2) and estimated maximum tornado wind speed (m/s). Coefficients of determination (R2) and regression equations are included as insets. See text for determination of (b) and (c), along with R2max and R2min values.

Using the mean radial length reduces the impact of outlier radial lengths, such that erroneously long (or short) radials might dramatically inflate (or deflate) the calculated OTA.

With GOES-16 data on OTs from observed storms (e.g., Figure 3), the analysis is restricted to a smaller portion of the domain that encompasses the track of the tornadic storm. The process begins by manually identifying the OT of the tornadic storm at the time of reported tornado formation within the LWIR imagery; no parallax correction is applied. This process is aided by Channel 2 visible satellite imagery, where available, and also uses Weather Surveillance Radar 88 Doppler (WSR-88D) radial velocity to ensure the correct OT is selected based upon the presence of a low-to-midlevel mesocyclone. Because of their manual identification, all OTs used here are relatively isolated, such that the we have high confidence that the OT is associated with the tornadic storm. The T_B data greater than the 25th percentile are masked, as this was found to eliminate nonanvil cloud tops within the cases of the anvil, thus highlighting the edges of the anvils. The inflection-based process is applied to the OT to quantify the OTA at this time (Figure 3). The OT is then tracked backward in time to 30 min prior to tornado formation using the location of T_{Bmin}, quantifying OTA using the process outlined above at each time. The OT is also tracked forward in time from reported formation to 30 min following reported tornado dissipation. This time window is employed to identify potential trends in these data during the processes of tornado formation and dissipation, to account for errors in reported formation time and to account for fluctuations in OTA that might correspond to periods of tornado intensification, as peak tornado intensity may not occur close to tornado formation (as might be the case for strong, long-track tornadoes). This results in a time series of OTA for the tornadic storm, from which the peak OTA is determined. Note that while the OTA time series are not analyzed further herein, future studies will include more detailed analysis of these data, with additional context provided by numerical simulations.

3. Results

As quantified by a linear regression analysis, stronger (higher EF-rated) tornadoes tend to be associated with larger peak OTA (Figure 4a; R^2 = 0.54, $p = 3.9 * 10^{-6}$). The regression analysis is supported by a box and whisker plot (Figure 5a), which shows a distinct separation between the OTA for relatively weaker tornadoes and the OTA for stronger tornadoes. A χ^2 test of independence further emphasizes the dependence of EF rating on OTA, indicating a significant relationship ($p = 2 * 10^{-4}$) between tornadoes rated EF3 and greater (EF2 and less) and OTA above (below) the overall mean OTA of 81.8 m^2.

As an aside, these results should be viewed in light of the well-established uncertainty associated with tornado EF ratings. Previous studies have established that use of damage surveys to estimate tornado intensity likely consistently underrates them (e.g., Alexander & Wurman 2008; Edwards et al., 2013). EF0 ratings are particularly problematic, as tornadoes can be assigned an EF0 rating based upon a lack of damage, meaning that tornadoes with actual wind speeds higher than those within the EF0 range are still rated as EF0. Although we have attempted to mitigate this uncertainty with the damage requirement outlined in section 2, it remains that many tornadoes rated EF0 may be significantly underestimated in their intensity (e.g., Doswell et al., 2009; Edwards et al., 2013).

We can, however, attempt to address some of the effect of this uncertainty on the OTA-tornado relationship with the following test. For cases with no reported wind speed estimate (see section 2), a wind speed within

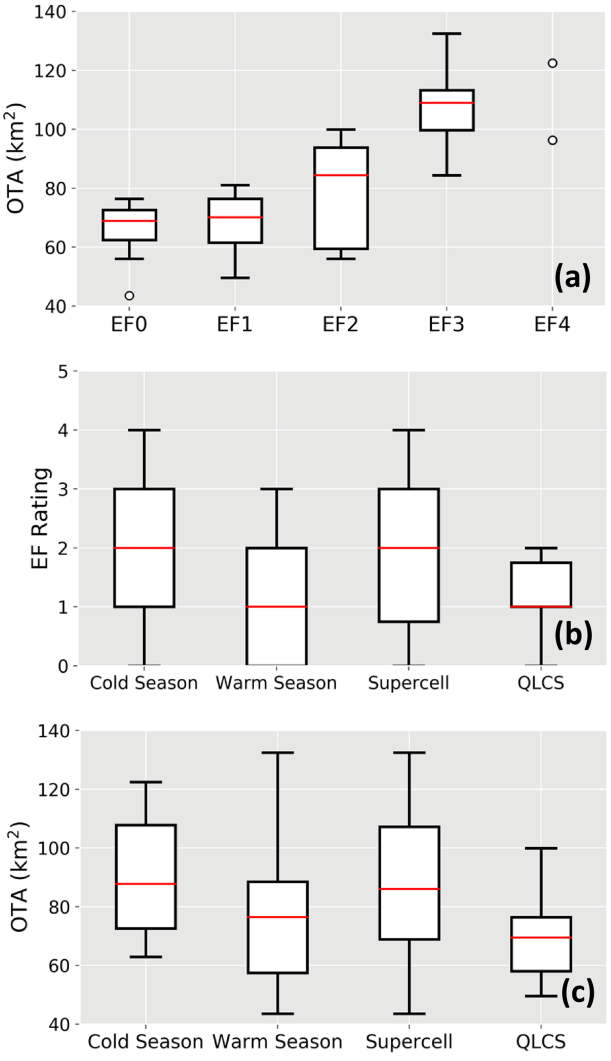

Figure 5. Box and whisker plot of (a) overshooting top area (OTA; km2) versus tornado Enhanced Fujita (EF) scale rating, (b) EF scale rating versus seasonal occurrence and storm morphology, and (c) OTA versus seasonal occurrence and storm morphology.

the assigned EF rating's wind range is randomly assigned. The regression analysis as in Figure 4a is then performed and R^2 value calculated. This process is repeated for 10^5 iterations, and the maximum and minimum R^2 values (R^2_{max} and R^2_{min}, respectively) for all iterations is determined. The analyses for the iterations with the R^2_{max} (=0.63) and R^2_{min} (=0.42) are shown in Figures 4b and 4c, respectively. Clearly, these serve to bracket well the original analysis in Figure 4a. More importantly, they indicate that a robust OTA-tornado relationship is realized even with uncertainties in wind speed assignments.

This relationship also does not appear to depend on the season or storm morphology of the cases examined. We find, for example, that the cool-season tornadic storms tend to have larger OTs than those of the warm-season tornadic storms. Although this might be counter to what one would expect, the cool season events considered here also have higher EF ratings than do the warm season events (Figure 5c). Note that "cool season" and "warm season" are defined simply by date, rather than by storm environments (e.g., as in Sherburn et al., 2016, who associated cool season tornado events with relatively low convective available potential energy and high vertical wind shear). In terms of storm morphology, we find somewhat expected results, with QLCS tornadoes (generally) having lower EF ratings (Figure 5c) and thus smaller OTAs (Figure 5b) than supercellular tornadoes (see also Figure 3). This implies support for the potential applicability to QLCS tornadoes of the conservation of circulation principle espoused by Trapp et al. (2017), further encouraging work on understanding intensity controls on these tornadoes.

This research was originally motivated by the desire to use GOES-R series data for severe-convective weather applications in operational settings. Although more cases are necessary to refine the OTA-EF relationship and thresholds, we can, at this point, conceive the following use of OTA as an estimator of potential tornado-intensity: Conditional on the formation of a tornado, the likelihood of the tornado becoming strong to violent (EF3–EF4) is higher when OTA $\geq$ 90 km^2, and the likelihood of it remaining weak to strong (EF0–EF2) is higher when OTA < 90 km^2. This simple OTA thresholding approach correctly categorizes 27 of our 30 tornado cases as either strong to violent (EF3–EF4) or weak to strong (EF0–EF2), providing additional motivation to pursue this further.

4. Discussion and Concluding Remarks

Our analysis of an initial GOES-16 LWIR data set shows support for the use of a proposed quantification of updraft area, namely, OTA, to identify storms with the highest potential to produce strong, damaging tornadoes. This statistically significant relationship between OTA and tornado intensity/EF is consistent with the theoretical and numerical modeling results of Trapp et al. (2017) and of ongoing Doppler-radar based quantifications (Sessa & Trapp, personal communication, 2019). The OTA-tornado relationship appears not to depend on seasonality or storm morphology.

We emphasize that our analysis herein assumes the existence of a tornado and, as such, is not intended to be used to anticipate *tornadogenesis* but rather *tornado intensity*. Because of this, we did not analyze nontornadic storms; however, future analysis will also include such null cases to determine if any differences between nontornadic and tornadic storms exist. Additional years of GOES-R series satellite operations will enable use of 1-min LWIR data to perform these analyses. These data will likely yield even better results given more accurate tracking of OTs, especially those associated with QLCSs, which tend to produce relatively short-lived tornadoes. Work is also ongoing to understand if and how OTA is related to and indicative of storm environmental characteristics, such as deep layer vertical wind shear and instability.

We highlight that the advantage of using geostationary satellites is mainly their continuous coverage over large portions of the world, including the contiguous United States. Ground-based weather radars, on the other hand, suffer from relatively sparse coverage in some locations, owing both to limitations in suitable radar sites and to beam blockage from complex terrain; these can be particularly problematic in parts of the eastern United States, which have active tornado seasons. The satellite-based approach proposed here does not suffer from these coverage limitations. Finally, this approach provides the opportunity for examining possible OTA-severe weather relationships (including for hail and severe wind intensity; e.g., Bedka et al., 2018; Punge et al., 2017) in other regions of the world, particularly those with little or no radar coverage.

The ultimate approach for the estimation of potential tornado intensity, however, is to use all data streams in tandem. Thus, our introduction of OTA here should improve upon the efforts of Smith et al. (2015), Thompson et al. (2017), and Cohen et al. (2018), who focused on the use of environmental and radar data for intensity estimation (see also Toth et al., 2013). In the spirit of Cohen et al. (2018), work is ongoing to develop a statistical model that accounts for OTA as well as pretornadic mesocyclone characteristics and evaluates the probable EF rating that a tornado will realize, should it form. This would provide a new tool for forecasters to communicate the relative risk of different tornado warnings to decision makers.

Acknowledgments
This research was supported by NOAA through Award NA17OAR4590195. Analyses were performed using open-source Python libraries NumPy and SciPy, with radar images produced using Py-ART (Helmus & Collis 2016). GOES-16 and WSR-88D data were obtained via NOAA's repository on Amazon S3. We are thankful for the helpful comments and recommendations of Michael French and one anonymous reviewer.

References

Adler, R. F., & Fenn, D. D. (1979). Thunderstorm intensity as determined from satellite data. *Journal of Applied Meteorology*, *18*(4), 502–517. https://doi.org/10.1175/1520-0450(1979)018<0502:TIADFS>2.0.CO;2

Adler, R. F., Fenn, D. D., & Moore, D. A. (1981). Spiral feature observed at top of rotating thunderstorm. *Monthly Weather Review*, *109*(5), 1124–1129. https://doi.org/10.1175/1520-0493(1981)109<1124:SFOATO>2.0.CO;2

Adler, R. F., Markus, M. J., & Fenn, D. D. (1985). Detection of severe Midwest thunderstorms using geosynchronous satellite data. *Monthly Weather Review*, *113*(5), 769–781. https://doi.org/10.1175/1520-0493(1985)113<0769:DOSMTU>2.0.CO;2

Alexander, C. W., & Wurman, J. (2008). Updated mobile radar climatology of supercell tornado structures and dynamics. Preprints, 24th Conf. on Severe Local Storms, Savannah, GA, American Meteorological Society, 19.4. Retreived from http://ams.confex.com/ams/pdfpapers/141821.pdf.]

Ashley, W. S. (2007). Spatial and temporal analysis of tornado fatalities in the United States: 1880–2005. *Weather and Forecasting*, *22*(6), 1214–1228. https://doi.org/10.1175/2007WAF2007004.1

Bedka, K., Brunner, J., Dworak, R., Feltz, W., Otkin, J., & Greenwald, T. (2010). Objective satellite-based detection of overshooting tops using infrared window channel brightness temperature gradients. *Journal of Applied Meteorology and Climatology*, *49*(2), 181–202. https://doi.org/10.1175/2009JAMC2286.1

Bedka, K., Murillo, E. M., Homeyer, C. R., Scarino, B., & Mersiovsky, H. (2018). The above-anvil cirrus plume: An important severe weather indicator in visible and infrared satellite imagery. *Weather and Forecasting*, *33*(5), 1159–1181. https://doi.org/10.1175/WAF-D-18-0040.1

Bedka, K. M., & Khlopenkov, K. (2016). A probabilistic multispectral pattern recognition method for detection of overshooting cloud tops using passive satellite imager observations. *Journal of Applied Meteorology and Climatology*, *55*(9), 1983–2005. https://doi.org/10.1175/JAMC-D-15-0249.1

Brooks, H. E. (2004). On the relationship of tornado path length and width to intensity. *Weather and Forecasting*, *19*(2), 310–319. https://doi.org/10.1175/1520-0434(2004)019<0310:OTROTP>2.0.CO;2

Brunner, J. C., Ackerman, S. A., Bachmeier, A. S., & Rabin, R. M. (2007). A quantitative analysis of the enhanced-V feature in relation to severe weather. *Weather and Forecasting*, *22*(4), 853–872. https://doi.org/10.1175/WAF1022.1

Cohen, A. E., Cohen, J. B., Thompson, R. L., & Smith, B. T. (2018). Simulating tornado probability and tornado wind speed based on statistical models. *Weather and Forecasting*, *33*(4), 1099–1108. https://doi.org/10.1175/WAF-D-17-0170.1

Doswell, C. A., Brooks, H. E., & Dotzek, N. (2009). On the implementation of the enhanced Fujita scale in the USA. *Atmospheric Research*, *93*(1–3), 554–563. https://doi.org/10.1016/j.atmosres.2008.11.003

Dworak, R., Bedka, K., Brunner, J., & Feltz, W. (2012). Comparison between GOES-12 overshooting-top detections, WSR-88D radar reflectivity, and severe storm reports. *Weather and Forecasting*, *27*(3), 684–699. https://doi.org/10.1175/WAF-D-11-00070.1

Edwards, R., LaDue, J. G., Ferree, J. T., Scharfenberg, K., Maier, C., & Coulbourne, W. L. (2013). Tornado intensity estimation: Past, present, and future. *Bulletin of the American Meteorological Society*, *94*(5), 641–653. https://doi.org/10.1175/bams-d-11-00006.1

Fujita, T. T. (1982). Principle of stereoscopic height computations and their applications to stratospheric cirrus over severe thunderstorms. *Journal of the Meteorology Society of Japan*, *60*(1), 355–368. https://doi.org/10.2151/jmsj1965.60.1_355

Goodman, S. J., Gurka, J., DeMaria, M., Schmit, T. J., Mostek, A., Jedlovec, G., Siewert, C., Feltz, W., Gerth, J., Brummer, R., Miller, S., Reed, B., & Reynolds, R. R. (2012). The GOES-R proving ground: Accelerating user readiness for the next-generation Geostationary Environmental Satellite System. *Bulletin of the American Meteorological Society*, *93*, 1029–1040. https://doi.org/10.1175/BAMS-D-11-00175.1

Helmus, J. J., & Collis, S. M. (2016). The Python ARM Radar Toolkit (Py-ART), a library for working with weather radar data in the Python programming language. *Journal of Open Research Software*, *4*(1), e25. https://doi.org/10.5334/jors.119

Homeyer, C. R., McAuliffe, J. D., & Bedka, K. M. (2017). On the development of above-anvil cirrus plumes in extratropical convection. *Journal of the Atmospheric Sciences*, *74*(5), 1617–1633. https://doi.org/10.1175/JAS-D-16-0269.1

Homeyer, C. R., Pan, L. L., & Barth, M. C. (2014). Transport from convective overshooting of the extratropical tropopause and the role of large-scale lower stratosphere stability. *Journal of Geophysical Research: Atmospheres*, *119*, 2220–2240. https://doi.org/10.1002/2013JD020931

McCann, D. W. (1983). The enhanced-V: A satellite observable severe storm signature. *Monthly Weather Review*, *111*(4), 887–894. https://doi.org/10.1175/1520-0493(1983)111<0887:TEVASO>2.0.CO;2

Mills, P., & Astling, E. (1977). Detection of tropopause penetrations by intense convection with GOES enhanced infrared imagery. *Preprints of the 10th Conference on Severe Local Storms*, Omaha, Nebraska: American Meteorology Society, 61–64.

Negri, A. J. (1982). Cloud-top structure of tornadic storms on 10 April 1979 from rapid scan and stereo satellite observations. *Bulletin of the American Meteorology Society*, *63*(10), 1151–1159. https://doi.org/10.1175/1520-0477-63.10.1151

Negri, A. J., & Adler, R. F. (1981). Relation of satellite-based thunderstorm intensity to radar-estimated rainfall. *Journal of Applied Meteorology*, *20*(3), 288–300. https://doi.org/10.1175/1520-0450(1981)020<0288:ROSBTI>2.0.CO;2

Punge, H. J., Bedka, K. M., Kunz, M., & Reinbold, A. (2017). Hail frequency estimation across Europe based on a combination of overshooting top detections and ERA-INTERIM reanalysis. *Atmospheric Research*, *198*, 34–43. https://doi.org/10.1016/j.atmosres.2017.07.025

Reynolds, D. W. (1980). Observations of damaging hailstorms from geosynchronous satellite digital data. *Monthly Weather Review*, *108*(3), 337–348. https://doi.org/10.1175/1520-0493(1980)108<0337:OODHFG>2.0.CO;2

Sherburn, K. D., Parker, M. D., King, J. R., & Lackmann, G. M. (2016). Composite environments of severe and nonsevere high-shear, low-CAPE convective events. *Weather and Forecasting*, *31*(6), 1899–1927. https://doi.org/10.1175/WAF-D-16-0086.1

Smith, B. T., Thompson, R. L., Dean, A. R., & Marsh, P. T. (2015). Diagnosing the conditional probability of tornado damage rating using environmental and radar attributes. *Weather and Forecasting*, *30*(4), 914–932. https://doi.org/10.1175/WAF-D-14-00122.1

Smith, B. T., Thompson, R. L., Grams, J. S., Broyles, C., & Brooks, H. E. (2012). Convective modes for significant severe thunderstorms in the contiguous United States. Part I: Storm classification and climatology. *Weather and Forecasting*, *27*(5), 1114–1135. https://doi.org/10.1175/WAF-D-11-00115.1

Thompson, R. L., Smith, B. T., Grams, J. S., Dean, A. R., Picca, J. C., Cohen, A. E., et al. (2017). Tornado damage rating probabilities derived from WSR-88D data. *Weather and Forecasting*, *32*(4), 1509–1528. https://doi.org/10.1175/WAF-D-17-0004.1

Toth, M., Trapp, R. J., Wurman, J., & Kosiba, K. A. (2013). Comparison of mobile-radar measurements of tornado intensity with corresponding WSR-88D measurements. *Weather and Forecasting*, *28*(2), 418–426. https://doi.org/10.1175/WAF-D-12-00019.1

Trapp, R. J., Marion, G. R., & Nesbitt, S. W. (2017). The regulation of tornado intensity by updraft width. *Journal of the Atmospheric Sciences*, *74*(12), 4199–4211. https://doi.org/10.1175/JAS-D-16-0331.1

Trapp, R. J., Marion, G. R., & Nesbitt, S. W. (2018). Reply to "Comments on 'The regulation of tornado intensity by updraft width'". *Journal of the Atmospheric Sciences*, *75*(11), 4057–4061. https://doi.org/10.1175/jas-d-18-0276.1

Trapp, R. J., Tessendorf, S. A., Godfrey, E. S., & Brooks, H. E. (2005). Tornadoes from squall lines and bow echoes. Part I: Climatological distribution. *Weather and Forecasting*, *20*(1), 23–34. https://doi.org/10.1175/WAF-835.1